Electronic Supplementary Material (ESI) for Journal of Materials Chemistry C.

Supporting Information for:

Optically switchable transistors comprising a hybrid photochromic molecule / *n-type* organic active layer

Karl Börjesson, Martin Herder, Lutz Grubert, Duc T. Duong, Alberto Salleo, Stefan Hecht, Emanuele Orgiu,* and Paolo Samorì**

Table of Contents

Synthesis

Details on the syntheses of **DAE-FN** and **DAE-F** according to Scheme S1 have been published recently.[1]

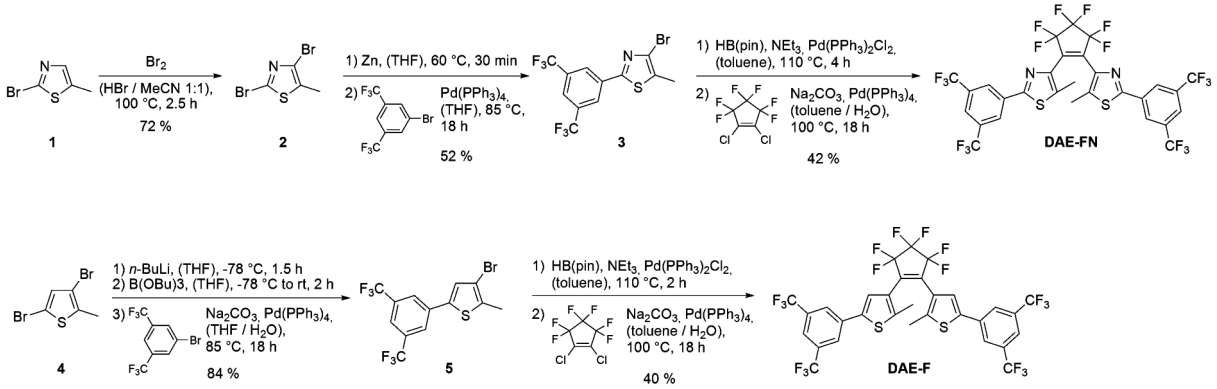

Scheme S1. Synthesis of **DAE-FN** and **DAE-F**.

Cyclic voltammetry

Cyclic voltammetry was performed using a PG310 USB (HEKA Elektronik) potentiostat interfaced to a PC with PotMaster v2x43 (HEKA Elektronik) software for data evaluation. A three-electrode configuration contained in a non-divided cell consisting of a platinum disc (d = 1 mm) as working electrode, a platinum plate as counter-electrode, and a saturated calomel electrode (SCE) with an agar-agar-plug in a Luggin capillary with a diaphragm as reference electrode was used. Measurements were carried out in acetonitrile (HPLC-grade, dried over calcium hydride and distilled) or acetonitrile/toluene (dried over sodium and distilled) containing 0.1 M Bu_4NPF_6 using a scan rate of dE/dt = 1 V s^{-1} or dE/dt = 0.1 V s^{-1}. The data is given in reference to the ferrocene redox couple (Fc/Fc^+), which was used as external standard. Cyclic voltammograms of ring-closed isomers of diarylethenes were obtained by irradiation of the electrochemical cell using a standard laboratory UV-lamp equipped with a 313 nm UV-tube. HOMO and LUMO levels are approximated from the measured anodic and cathodic peak potentials using an energy level of ferrocene/ferrocenium of 4.8 eV below vacuum.[2, 3]

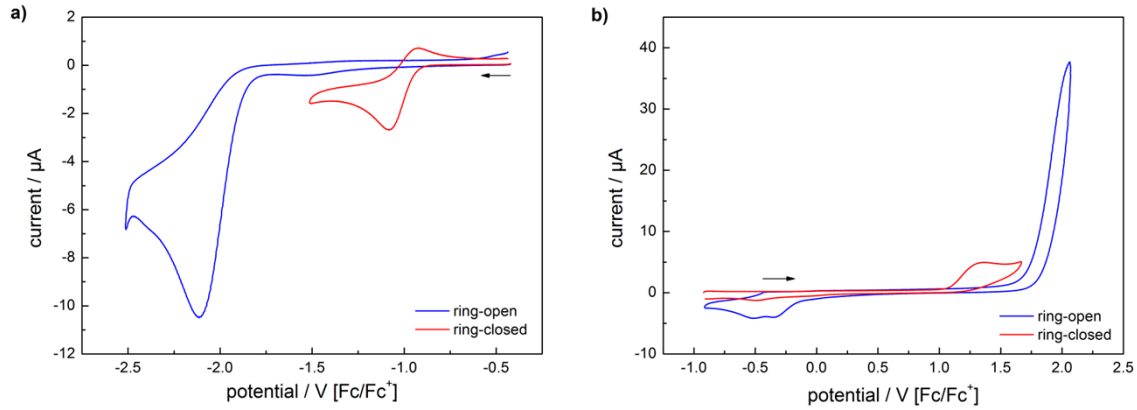

Figure S1. Cyclic voltammetry of **DAE-FN** (c = $1 \cdot 10^{-3}$ M) in acetonitrile (0.1 M Bu_4NPF_6): a) reduction, b) oxidation, dE/dt = 1 V s^{-1}.

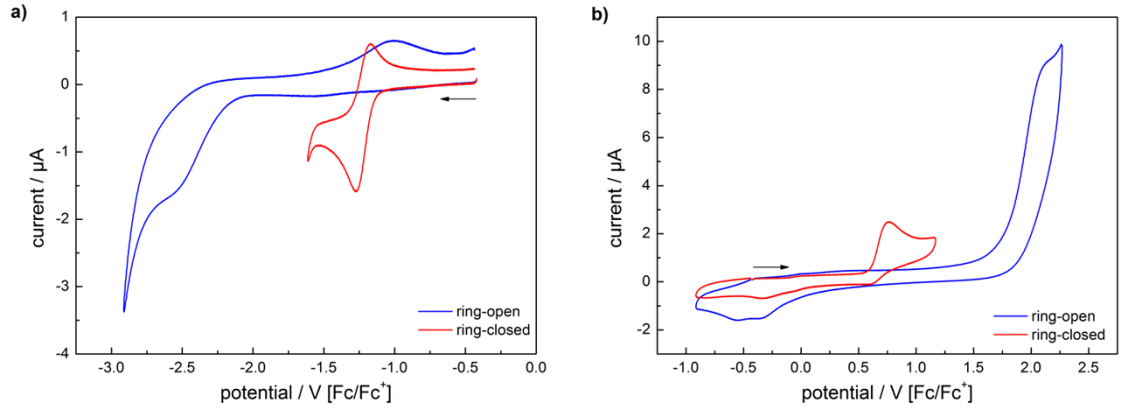

Figure S2. Cyclic voltammetry of **DAE-F** (c = $1 \cdot 10^{-3}$ M) in acetonitrile (0.1 M Bu_4NPF_6): a) reduction, b) oxidation, dE/dt = 1 V s^{-1}.

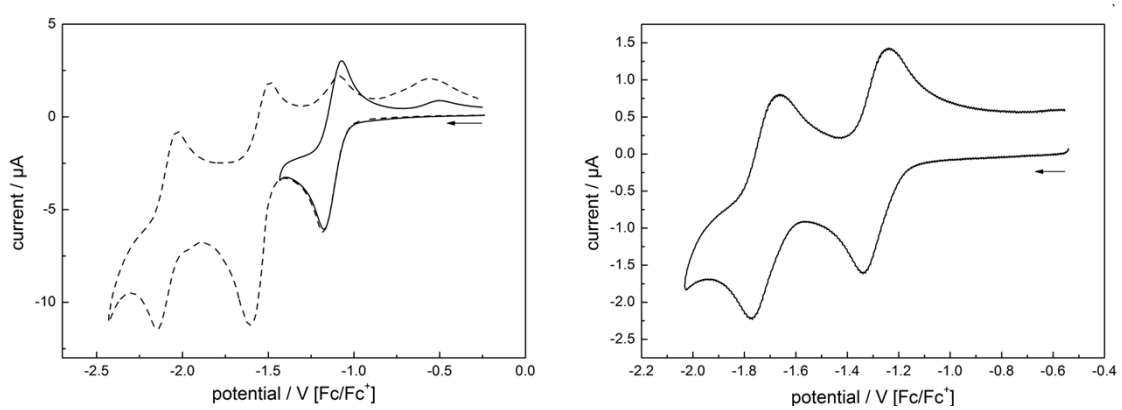

Figure S3. Left: Cyclic voltammetry of **PCBM** (c = $1 \cdot 10^{-3}$ M) in toluene/acetonitrile 3:1 (0.1 M Bu_4NPF_6), dE/dt = 0.1 V/s. Right: Cyclic voltammetry of **ICBA** (c = $5 \cdot 10^{-4}$ M) in toluene/acetonitrile 3:1 (0.1 M Bu_4NPF_6), dE/dt = 0.1 V/s.

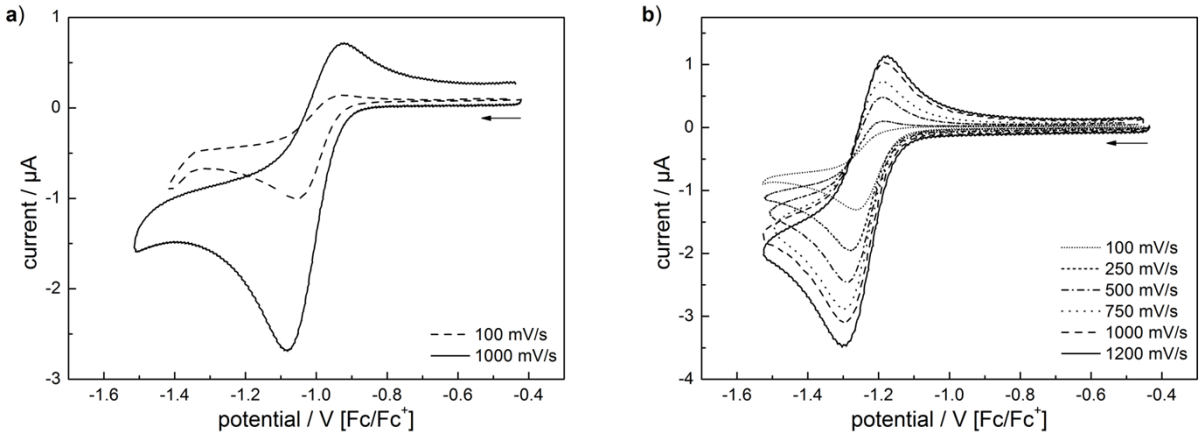

Figure S4. Scan rate dependence of the first reduction wave of the ring-closed isomer of a) **DAE-FN** and b) **DAE-F** in acetonitrile (0.1 M Bu_4NPF_6). While the reductions are irreversible at low scan rates, they become reversible upon higher scan rates. The shift of the peak potentials upon varying scan rates is significantly smaller than the relative difference between the reduction potentials of the two DAEs.

Table S1. Oxidation and reduction peak potentials and derived HOMO/LUMO levels of **DAE-FN, DAE-F, PCBM,** and **ICBA**.

	E_p^{a1} [V] vs. Fc/Fc^+	HOMO [eV][a]	E_p^{c1} [V] vs. Fc/Fc^+	LUMO [eV][a]
DAE-FN_o[b]	> 2.00	< -6.80	-2.11	-2.69
DAE-FN_c[b]	1.35	-6.15	-1.08	-3.72
DAE-F_o[b]	> 2.00	< -6.80	-2.56	-2.24
DAE-F_c[b]	0.76	-5.56	-1.27	-3.53
PCBM[c]	-	-	-1.18	-3.62
ICBA[c]	-	-	-1.37	-3.43

[a] $E^{HOMO/LUMO} = -e\, E_p^{a1/c1}(Fc/Fc^+) - 4.8$ eV

[b] acetonitrile

[c] toluene/acetonitrile 3:1

Photochemistry in solution

UV/vis spectroscopy was performed on a Cary50 spectrophotometer equipped with a Peltier thermostated cell holder at 25 °C. Irradiation experiments were carried out with a 1000 W high pressure Xe lamp. Wavelength selection was achieved using an interference filter (Asahi Spectra, 50 % transmission at λ_{max} = 310 nm, FWHM = 10 nm) for UV light irradiation and a cutoff filter (80 % transmission for λ > 500 nm) for visible light irradiation. Conversion to the ring-closed isomer in the photostationary state (PSS) was determined by injection of irradiated samples into a UPLC (solvent gradient acetonitrile/water) and integration of the diode array signal at the isosbestic wavelength. Spectra of pure ring-closed isomers were calculated from spectra of the PSS and the determined composition.

Quantum yields were determined by photokinetic measurements performed using a LOT-Oriel 500 W Hg(Xe) lamp coupled to a LOT-Oriel monochromator equipped with a timed shutter. The light output of the lamp setup was transferred to the cell compartment of a Cary 60 spectrophotometer using an optical fiber. The irradiation beam was assembled orthogonal to the measurement beam of the spectrophotometer to enable simultaneous irradiation and probing of a 3 mL quartz cuvette in a thermostated cell holder at 25 °C. During photokinetic measurements effective stirring of the sample was ensured. Actinometry was performed using ferrioxalate[4] for UV irradiation and Aberchrome 670[5] for visible light irradiation.

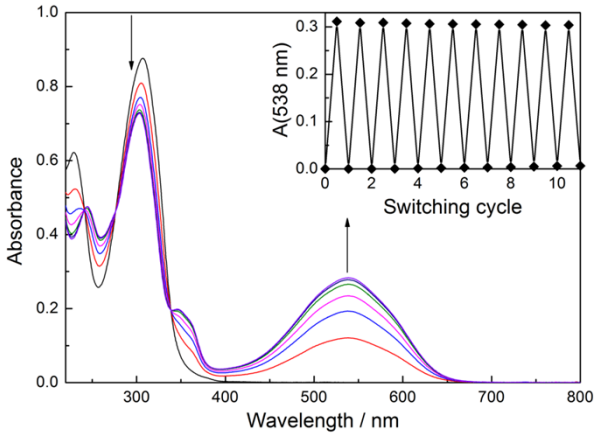

Figure S5. UV/vis spectra during the course of irradiation of solutions of **DAE-FN** in acetonitrile ($c = 2.8 \cdot 10^{-5}$ M) with UV-light (λ_{irr} = 310 nm) until reaching the photostationary state. Inset: Repetive irradiation with UV (λ_{irr} = 310 nm) and visible light (λ_{irr} > 500 nm).

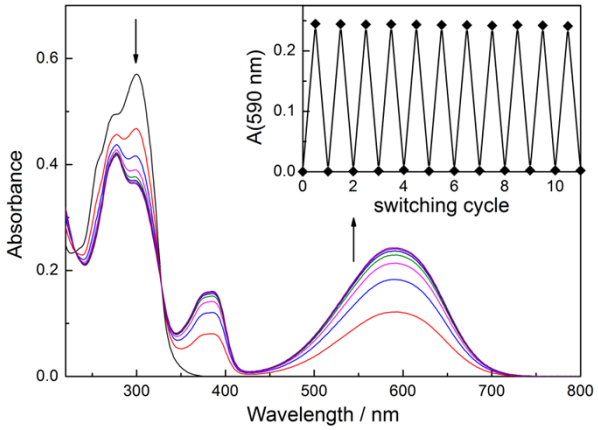

Figure S6. UV/vis spectra during the course of irradiation of solutions of **DAE-F** in acetonitrile ($c = 1.7 \cdot 10^{-5}$ M) with UV-light (λ_{irr} = 310 nm) until reaching the photostationary state. Inset: Repetive irradiation with UV (λ_{irr} = 310 nm) and visible light (λ_{irr} > 500 nm).

Table S2. Photochromic properties of **DAE-FN** and **DAE-F** in acetonitrile.

	λ_{max} / nm (ε / 10^4 M^{-1} cm^{-1})	$\Phi_{o\rightarrow c}$ (313 nm)	$\Phi_{c\rightarrow o}$ (546 nm)	PSS[a]
DAE-FN_o	307 (3.11)	0.45	0.04	89%
DAE-FN_c	303 (2.52), 538 (1.13)			
DAE-F_o	300 (3.45)	0.58	0.02	96%
DAE-F_c	277 (2.51), 590 (1.54)			

[a] Conversion to the closed isomer upon UV irradiation in the photostationary state.

Preparation of organic thin-film transistors

Bottom-gate bottom-contact transistors were fabricated on heavily doped n-type silicon wafers serving as a gate electrode with 230-nm thick thermally-grown SiO_2 as the dielectric layer (C_i=15 nF/cm^2) having pre-patterned gold electrodes (IPMS Fraunhofer). The oxide surface was functionalized with hexamethyldisilazane (HMDS).The chips were cleaned by ultrasonication first in acetone and then in propanol. In order to improve the injection of electrons from a high work-function metal (Au) into a *n*-type semiconductor, the source and drain electrodes were functionalized via immersion in a 0.5 mM 1-undecanethiol solution (ethanol) overnight in N_2 atmosphere. Pristine semiconductors or semiconductor/DAE blends (blend ratio 5/1 weight, in all cases) were spin-coated from chlorobenzene solution (10 and 20 mg/ml, spin-coated at 500 and 800 rpm, for PCBM and ICBA devices, respectively) on the transistor substrates which underwent the functionalization of both oxide and electrodes (as described above) in N_2 atmosphere (glovebox). Electrical characterization of the devices was performed at room temperature in a N_2 atmosphere inside the glovebox, using a Cascade Microtech M150 probe station and a Keithley 2636A controlled by Labtracer$^{(TM)}$ software.

Parameter extraction and data

The drain current of a field-effect transistor can be correlated with the applied bias voltages to the gate and drain electrodes through Equation S1 (when working in the saturation regime, where $V_D \geq V_G - V_{th}$)[6]

$$I_D = \frac{1}{2}\mu_{SAT} C_i \frac{W}{L}(V_G - V_{th})^2 \qquad \text{Equation S1}$$

Where I_D is the drain current, V_G the gate voltage, V_D the drain voltage, L the channel length, and C_i=1.5·10^{-8} F·cm^{-2} the capacitance of the gate dielectric per unit area. The field-effect mobility can then be extracted using Equation S2.

$$\mu_{SAT} = \frac{2\left(\frac{\partial\sqrt{I_D}}{\partial V_G}\right)}{C_i \frac{W}{L}} \qquad \text{Equation S2}$$

Threshold voltage, V_{th}, values were calculated by plotting the $I_D^{0.5}$ vs. V_G curve and then extracting the intercept with the voltage axis of the line which fits the linear part of the curve. The threshold voltages as well as field-effect mobilities are summarized in Figure S7, and examples of I_D vs. V_G curves before and after UV illumination are shown in Figure S8. A channel length of 10 µm was used if not otherwise stated.

The following standard procedure was used when measuring the switching efficiency as shown in Figure 3. The reason for the higher irradiation time and power in the visible region is due to the lower photoisomerization quantum yield for the closed to open isomerization (see table S2). Point 0 is the starting current value measured before any kind of irradiation i.e. in the dark.

1. Irradiation at 320 nm (180 µW/cm²) for 30 s followed by 30 s in dark (indicated by violet in Figure 3). The value of drain current at V_D = 40 V and V_G = 80 V for ICBA and V_G = 120 V for PCBM based transistors is taken from the full I_D - V_G curve.

2. Irradiation at 540 nm (8.2 mW/cm²) for 10 min followed by 30 s in dark (indicated by green in Figure 3). The value of drain current at V_D = 40 V and V_G = 80 V for ICBA and V_G = 120 V for PCBM based transistors is taken from the full I_D - V_G curve.

3. Point 1 and 2 was continuously repeated.

4. For repeated readouts without irradiation in between (Entry 7-8, 9-10, 11-13, and 14-16 in Figure 3) the time between measurements were 30 s.

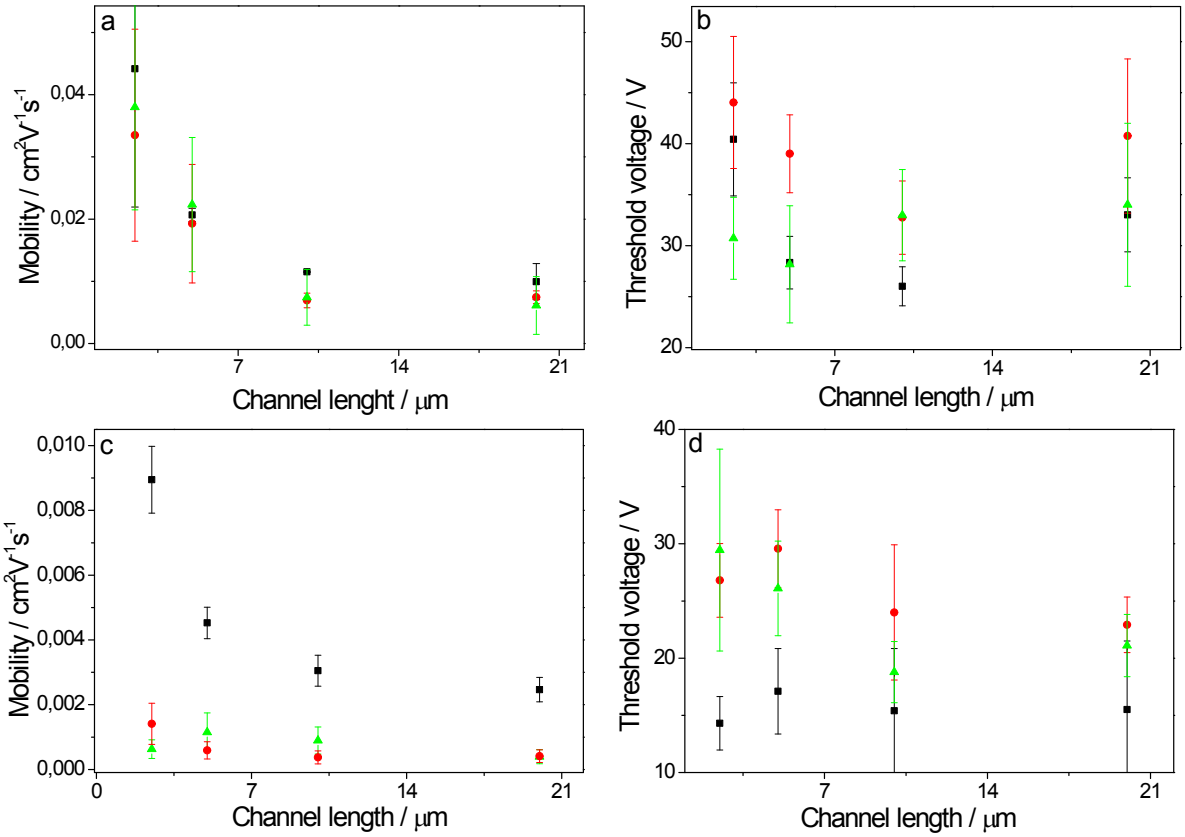

Figure S7. Field-effect mobilities and threshold voltages of PCBM (a and b) and ICBA (c and d) based devices (black squares=pristine semiconductor, red circle=DAE-FN blend, green triangle=DAE-F blend).

Table S3. Number of transistors analyzed to generate the data presented in Figure S7 and Table 1.

Channel length	PCBM	PCBM/DAE-FN	PCBM/DAE-F	ICBA	ICBA/DAE-FN	ICBA/DAE-
2.5 µm	4	4	8	7	9	6
5 µm	4	4	7	7	6	6
10 µm	4	3	7	8	8	5
20 µm	5	4	7	8	7	4

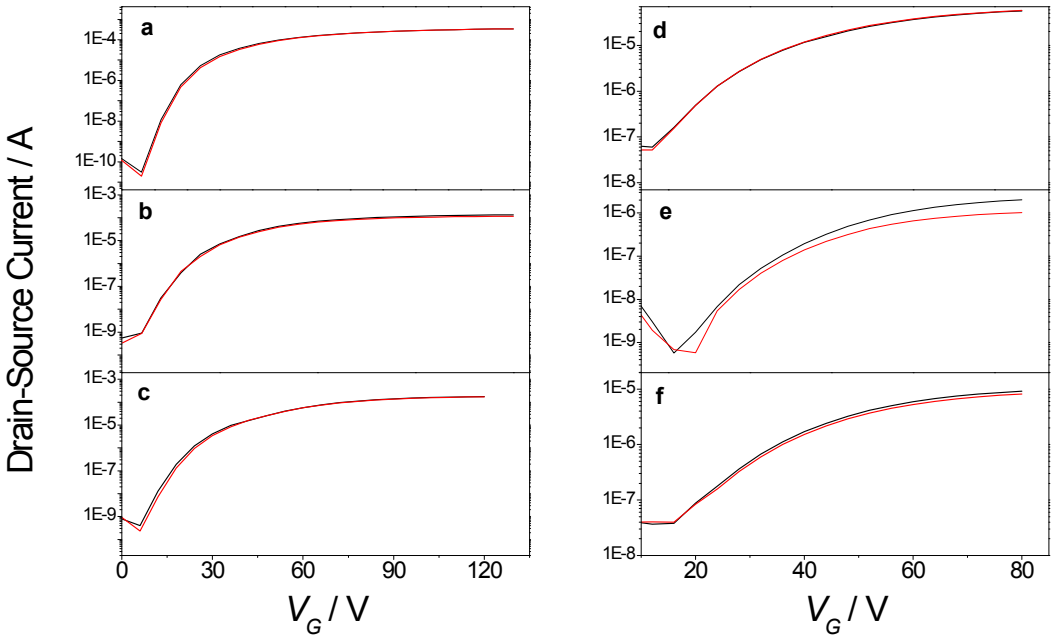

Figure S8. Examples of I_D vs. V_G sweeps before (black) and after (red) switching from the open to the closed form by irradiation at 320 nm for pristine PCBM (a), PCBM/DAE-FN blend (b), PCBM/DAE-F blend (c), pristine ICBA (d), ICBA/DAE-FN blend (e), and ICBA/DAE-F blend (f; Same dataset as in Figure 3 but plotted in log scale).

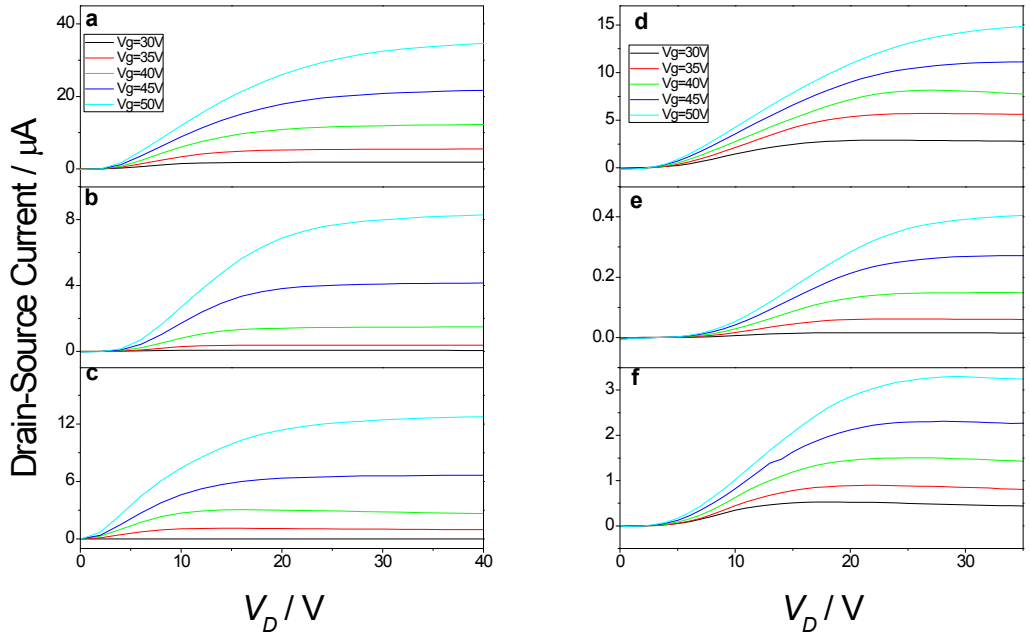

Figure S9. Examples of I_D vs. V_D sweeps for pristine PCBM (a), PCBM/DAE-FN blend (b), PCBM/DAE-F blend (c), pristine ICBA (d), ICBA/DAE-FN blend (e), and ICBA/DAE-F blend (f)

Table S4. I_{On}/I_{off} ratios for transistors in Figure S8.

Compound	I_{On}/I_{off} ratio
PCBM	$1.8 \cdot 10^7$
PCBM/DAE-FN	$3.5 \cdot 10^5$
PCBM/DAE-F	$4.2 \cdot 10^5$
ICBA	$9.7 \cdot 10^2$
ICBA/DAE-FN	$3 \cdot 10^3$
ICBA/DAE-F	$2.5 \cdot 10^2$

Analysis of degradation upon switching

To gain further insights if the lower switching fatigue resistance of the ICBA than PCBM blended transistors is due to the degradation of the photochromic molecules or to that of the semiconductor, the current switching efficiency as a function of number of switches, and the degradation of pristine semiconductor devices were analyzed. Table S3 shows the switching cycle efficiency (same dataset as in Figure 3 in main article) and it reveals that no difference in the cycle efficiency with respect to number of switching cycles is observed between ICBA and PCBM blended devices. For pristine ICBA and PCBM devices, a decrease in current of 9 and 6 %, respectively, could be observed after 5 complete switching cycles and 17 transfer sweeps. Furthermore, when examining the bias stress of pristine ICBA and PCBM devices (Figure S9), it is clear that PCBM devices have a higher tolerance to bias stress than ICBA devices. The conclusion is therefore that the lower fatigue resistance of switching of ICBA/DAE blended devices mainly is due to degradation of semiconductor and cannot be ascribed to the photochromic compound.

Table S5. The switching cycle efficiency for each individual open to closed switch is here presented using the same dataset as in Figure 3 in the main article (calculated as the source drain current after open→closed isomerization divided by current before isomerization).

Compound	Switch 1	Switch 2	Switch 3	Switch 4	Switch 5	Average (std)
PCBM	1.00	1.00	1.00	1.00	1.00	1.00
PCBM/DAE-FN	0.86	0.86	0.87	0.88	0.89	0.87 (0.012)
PCBM/DAE-F	0.97	0.97	0.98	0.99	0.99	0.98 (0.009)
ICBA	1.02	1.01	1.01	1.00	1.01	1.01 (0.006)
ICBA/DAE-FN	0.45	0.47	0.49	0.49	50	0.48 (0.018)
ICBA/DAE-F	0.89	0.89	0.88	0.90	0.91	0.89 (0.01)

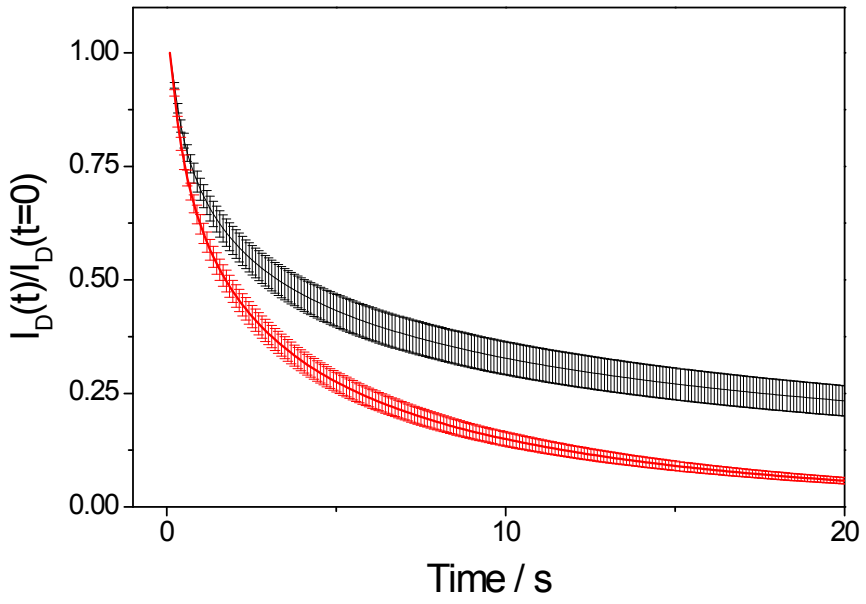

Figure S10. Bias stress of PCBM (black) and ICBA (red) devices. To accurately compare the two semiconductors, the gate voltages for each tested device was biased relative to the threshold voltage of that device ($V_G=V_{th}+50$), and the drain source voltage was set to 40 V.

AFM characterization

AFM was performed on the same transistors chips as used for the electrical characterization experiments. A Veeco Dimension 3100 AFM running with a Nanoscope IV controller was used. AFM images were recorded in the intermittent contact (tapping) mode under ambient conditions using standard silicon cantilevers (Veeco MPP-11120-10).

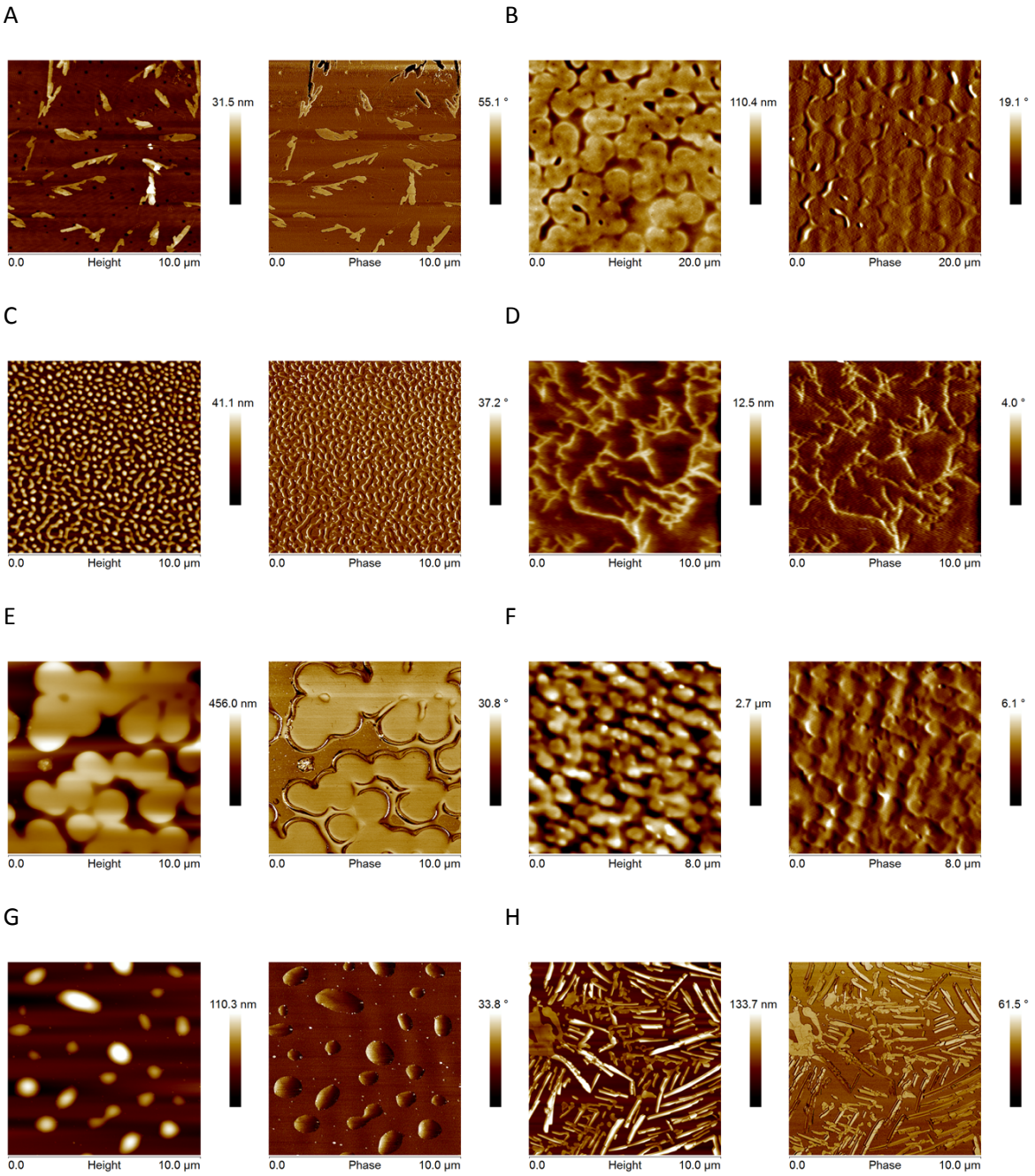

Figure S11. AFM images of spin-coated films of pristine PCBM (A), PCBM/DAE-FN (B), PCBM/DAE-F (C), pristine ICBA (D), ICBA/DAE-FN (E), ICBA/DAE-F (F), and drop-cast films of pristine DAE-FN (G), and pristine DAE-F (H). The films of pristine PCBM and ICBA show a relatively smooth surface with what appears as crystal formation on the surface, whereas the blended films have clear tendencies of phase segregation.

Microstructure characterization of neat and blended films by 2D Grazing Incidence X-ray Diffraction (2D-GIXD)

2D-GIXD was performed on the same transistors samples as used for the electrical characterization experiments. Diffraction patterns are collected using synchrotron radiation at the Stanford Synchrotron Radiation Lightsource (SSRL). Experiments were carried out with an incident beam of 12.7 keV at a grazing angle of 0.1° and expressed as a function of the scattering vector $q = 4\pi\sin(\vartheta)/\lambda$. Here ϑ represents half of the scattering angle, λ is the wavelength of the incident beam, q_{xy} is the component of the scattering vector parallel to the substrate plane and q_z is the component perpendicular to the substrate plane.

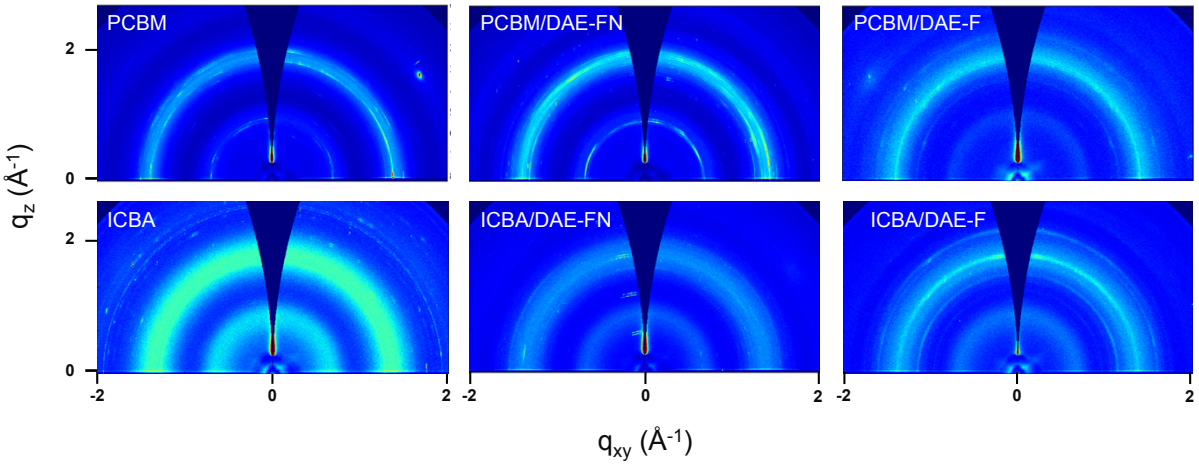

Figure S12. Two-dimensional grazing-incidence X-ray diffraction on PCBM, ICBA, DAE-FN, and DAE-F blended films. All films are to a high degree amorphous.

Characterization of phase separation in neat and blended films by Scanning Auger Microscopy

Scanning electron microscopy (SEM) and auger microscopy were performed on a PHI 700 Scanning Auger Nanoprobe at an accelerating voltage of 10kV.

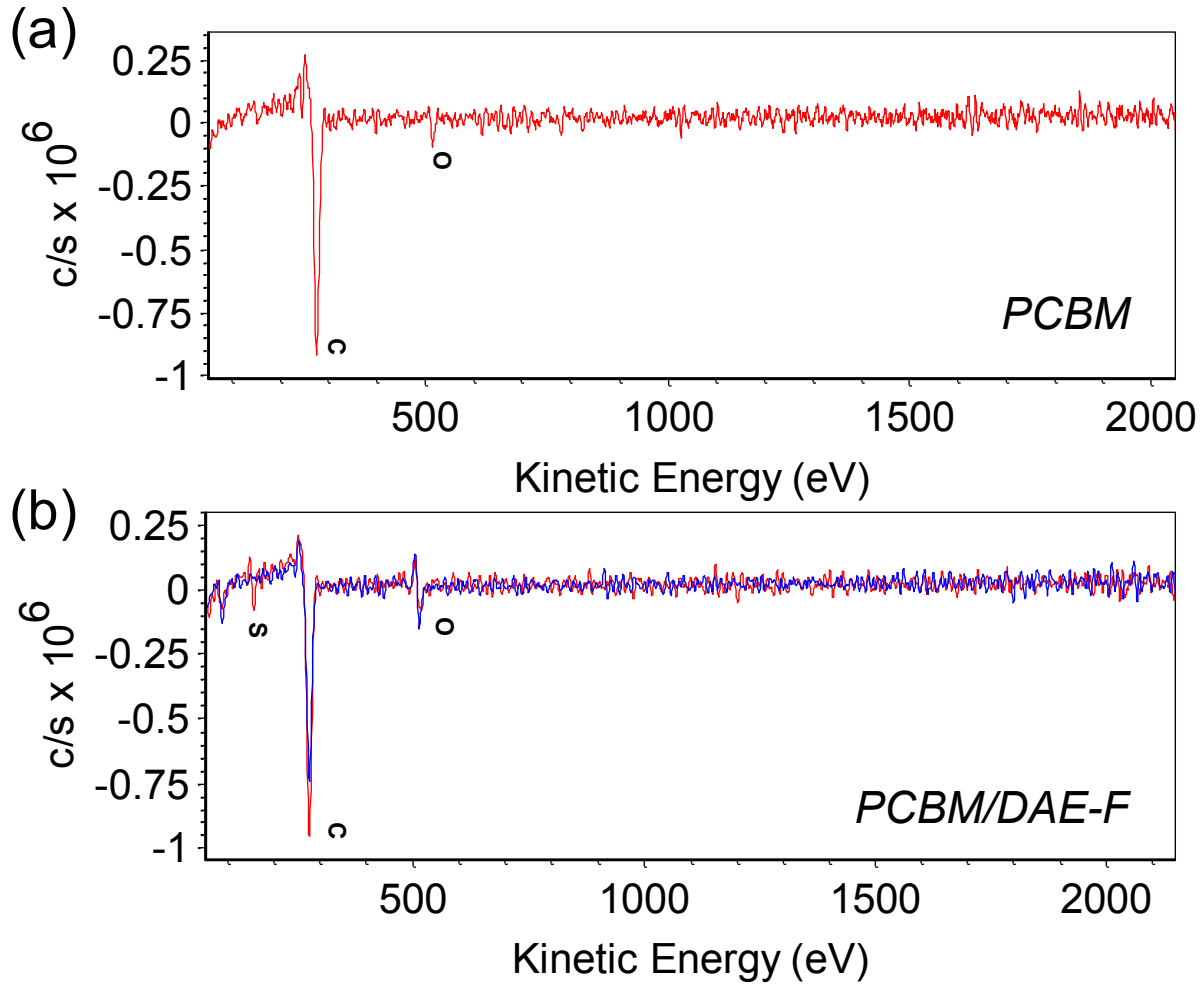

Figure S13. Representative Auger spectra for (a) PCBM and (b) PCBM/DAE-F. As shown, only carbon (C) and (O) can be detected in the pure fullerene film whereas blended films also contain sulfur (S). Although there are also nitrogen and fluorine atoms in the DAE molecules, their signals are too weak to be detected here.

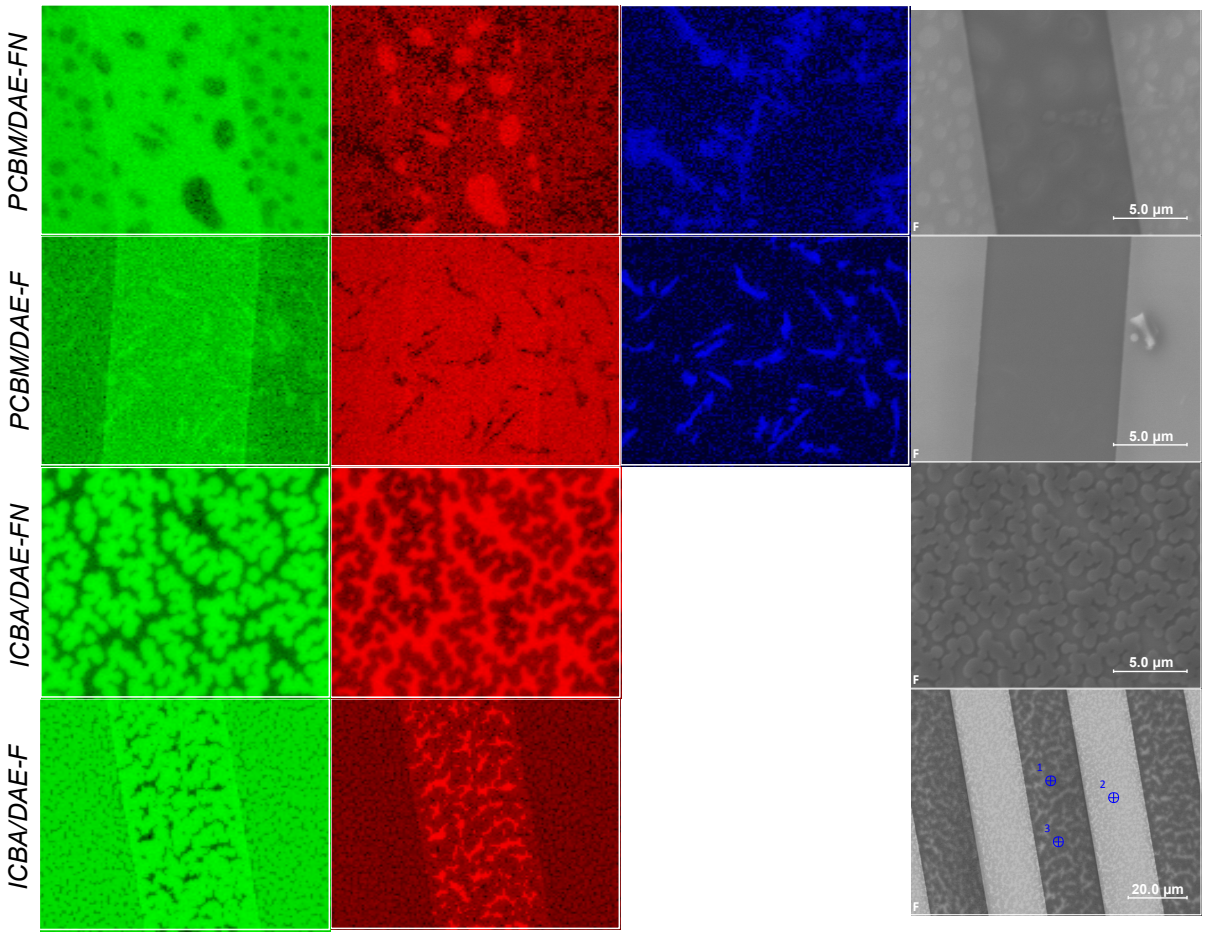

Figure S14. Auger and electron microscopy map for blend films of ICBA, PCBM and DAE molecules. Carbon (green), oxygen (red), sulfur (blue) and SEM images are shown here at a scan size of 20x20 µm. For ICBA/DAE-F, however, carbon and oxygen maps are 50x50 µm in size and the corresponding SEM image is 100x100 µm in size. As shown, sulfur signals are only detected in the PCBM blends and not in the ICBA blends (hence the missing sulfur map). In the case of PCBM blends, sulfur signals appear as large, micron-sized aggregates. From this we conclude that PCBM/DAE films exhibit more phase separation than ICBA/DAE films, where DAE molecules are probably embedded inside the ICBA aggregates and cannot be detected by Auger spectroscopy, which only probes up to ~5 nm into the film. This explains why we see reduced field-effect mobility in ICBA/DAE blends.

References

1 M. Herder, B. M. Schmidt, L. Grubert, M. Pätzel, J. Schwarz and S. Hecht, *J. Am. Chem. Soc.*, 2015, **137**, 2738-2747.

2 J. Pommerehne, H. Vestweber, W. Guss, R. F. Mahrt, H. Bässler, M. Porsch and J. Daub, *Adv. Mater.*, 1995, **7**, 551-554.

3 C. M. Cardona, W. Li, A. E. Kaifer, D. Stockdale and G. C. Bazan, *Adv. Mater.*, 2011, **23**, 2367-2371.

4 C. G. Hatchard and C. A. Parker, *Proc. R. Soc. London, Ser. A*, 1956, **235**, 518-536.

5 A. P. Glaze, H. G. Heller and J. Whittall, *J. Chem. Soc. Perk. Trans. 2*, 1992, 591-594.

6 G. Horowitz, R. Hajlaoui, H. Bouchriha, R. Bourguiga and M. Hajlaoui, *Adv. Mater.*, 1998, **10**, 923-927.